Deep-Sea Research II 77–80 (2012) 89–98

Contents lists available at SciVerse ScienceDirect

Deep-Sea Research II

journal homepage: www.elsevier.com/locate/dsr2

Trends in the surface chlorophyll of the California Current: Merging data from multiple ocean color satellites

Mati Kahru [a,*], Raphael M. Kudela [b], Marlenne Manzano-Sarabia [c], B. Greg Mitchell [a]

[a] Scripps Institution of Oceanography, University of California San Diego, La Jolla, California, USA
[b] Ocean Sciences Department, University of California Santa Cruz, Santa Cruz, CA 95064, USA
[c] Facultad de Ciencias del Mar, Universidad Autónoma de Sinaloa, Mazatlán, Sinaloa, México

ARTICLE INFO

Available online 24 April 2012

Keywords:
Ocean color
Phytoplankton
Chlorophyll
California Current
Remote sensing

ABSTRACT

Standard remote sensing reflectance products from four ocean color sensors (OCTS, SeaWiFS, MODISA, MERIS) and over 10,000 in situ measurements of surface chlorophyll-a (*Chl-a*) concentration in the California Current were used to create empirical algorithms that are consistent with in situ data as well as between individual sensors. Using these algorithms, a merged multi-sensor time series of the surface *Chl-a* concentration in California Current region was created. The merged *Chl-a* time series (November 1996–December 2011) show a significant ($P<0.01$) increasing trend off central California and significant ($P<0.01$) decreasing trends in the central North Pacific gyre and off southern Baja California. Although this 15-year time series is too short to separate interannual and multidecadal cycles from climate trends, both of these trends are consistent with the predicted effects of global warming. The expected increase in vertical stratification of the water column and the resulting decreased vertical flux of nutrients would lead to lower *Chl-a* in the gyre but the increased upwelling-favorable winds leading to stronger upwelling off central California or the increased nitrate content of the upwelled water would lead to higher *Chl-a* in the upwelling region. The decreased *Chl-a* off southern Baja California resembles the effect of a decreased influence of strong El Nino events.

1. Introduction

Oceanic phytoplankton plays an important role in global carbon and energy budgets and any changes in its composition and/or concentration are therefore of special interest, especially in the context of the global climate change debate. A claim by Boyce et al. (2010) that global phytoplankton biomass has lost over 60% of its value over the last 100 years (i.e. a loss of 1% per year) has been challenged by others (Mackas, 2010; McQuatters et al., 2011; Rykaczewski and Dunne, 2011). It is obvious that traditional ship-based sampling does not have the required spatial coverage and temporal frequency to reliably detect global long-term changes in the patchwork of regionally varying increases and decreases with a multitude of forcings at seasonal, interannual and decadal scales (Martinez et al., 2009). Satellite observations of ocean color have the potential to better detect long-term trends due to their greatly improved temporal frequency and almost global coverage but are limited by their relatively short duration and uncertainties associated with instrument calibration and data processing algorithms (McClain, 2009). As the life-span of a single satellite sensor is limited, a major task is to seamlessly merge data from multiple satellite sensors that have different optical bands, sensitivities, noise patterns and overpass times (Maritorena and Siegel, 2005). Even relatively similar sensors like MODIS on Terra and MODIS on Aqua (see Tables A1 and A2 for acronyms and notations) have very different sensor characteristics in addition to the different orbits. Merging data from multiple sensors to a single unified time series that qualifies as a climate data record (National Research Council, 2004) remains a major challenge (Gregg et al., 2009). While great improvements have been made in on-orbit assessment of alterations in sensor characteristics over time, atmospheric correction and sensor calibration procedures (Franz et al., 2007), these may not be enough to create continuous climate data records due to the extreme sensitivity of the detection of in-water properties to various sensor calibration errors as well as to differences in orbits (Gregg et al., 2009).

The California Current is a major and well-characterized Eastern boundary current with research programs such as CalCOFI (Mantyla et al., 1995) going back many decades. While the primary expected response to increased surface warming of the ocean is increased stratification and decreased primary productivity, studies in the California Current have reported the opposite trends: increasing turbidity (Aksnes and Ohman, 2009) and

* Corresponding author. Tel.: +1 858 534 8947; fax: +1 858 822 0562.
E-mail address: mkahru@ucsd.edu (M. Kahru).

0967-0645/$ - see front matter © 2012 Elsevier Ltd. All rights reserved.
http://dx.doi.org/10.1016/j.dsr2.2012.04.007

increasing surface chlorophyll-a (*Chl-a*) and primary productivity in the coastal zone (Kahru et al., 2009). It is clear that the complex interactions between surface warming on one hand and wind forcing and upwelling on the other hand are difficult to predict and much more analysis is needed.

Here we use over 10,000 *Chl-a* samples collected by various research programs in the California Current during the period when high-quality data from ocean color satellite sensors have been available. We create satellite algorithms that are empirically tuned to the in situ *Chl-a* datasets and minimize the inter-sensor differences at the same time. We then merge satellite data from four ocean color sensors (OCTS, SeaWiFS, MODISA and MERIS) into a unified time series of surface *Chl-a* and evaluate trends during the last 15 years (1996–2011).

2. Data and methods

2.1. In situ data

Various data sources for surface *Chl-a* data are listed in Table A3. The total number of near-surface *Chl-a* samples that were used to validate satellite data in 1996–2010 was 10,050 (Table 1), i.e. about 670 *Chl-a* stations per year. For each station the sample nearest to the surface (typically 1–10 m) was used. This included only the high-quality datasets with at least one station far enough from the coast to provide at least 7 valid pixels in the 3×3 pixel window centered at the in situ sample location. Data from several near-shore projects were excluded as they were too close to the shore to have any refined satellite match-ups. A few other datasets were excluded due to questionable calibration accuracy and sample collection procedures. Most of the in situ *Chl-a* data (*Cins*, mg m^{-3}) were obtained with the standard fluorometric method (Lorenzen, 1981). Fluorometric *Chl-a* values were replaced with total *Chl-a* when measurements with the more accurate HPLC method were available. A comparison of the *Chl-a* measurements made with the fluorometric and HPLC methods showed very high correlation with a slope close to one and an intercept not distinguishable from zero. The linear regression between log 10-transformed values was $Chl_{HPLC} = -0.056 + 0.988 Chl_{Fluor}$, $r^2 = 0.97$, $RMSE = 0.09$, $N = 838$.

2.2. Match-ups between satellite and in situ data

The validation of satellite products using quasi-simultaneous and spatially collocated measurements (match-ups) of satellite and in situ data followed the general procedures of previous studies (e.g. Kahru and Mitchell, 1999; Werdell and Bailey, 2005; Bailey and Werdell, 2006; Antoine et al., 2008). As the spatial resolution of a typical ocean color satellite sensor is about 1 km at nadir viewing, it is practically impossible to find areas in the California Current that are spatially uniform within the footprint of a satellite pixel. Due to navigational errors in the satellite and in situ sampling as well as the movement of the water parcel during the time lag between the satellite pass and the in situ sample, the value of the nearest pixel is not always the best match. We therefore used statistics of a set of 3×3 pixels of satellite data centered at the location of the in situ sample as the match-up for the in situ sample. The latest available versions of data from four different satellite sensors were used (see http://oceancolor.gsfc.nasa.gov/WIKI/OCReproc.html for details): 2010.0 for OCTS, 2010.1 for SeaWiFS (1997–2010), 2009.1 (2002–2008) and 2010.0 (2009–2011) for MODISA, 2nd reprocessing for MERIS (2003–2010). For SeaWiFS and MODISA we used the full resolution ($\sim$1 km) Level-2 data. For OCTS and MERIS we used the reduced resolution Level-2 data, i.e., GAC ($\sim$4 km) data for OCTS and RR data ($\sim$1 km) for MERIS. For OCTS each GAC pixel is every 4th full resolution pixel both along and across the track of the satellite with a ground separation of about 4 km. The MERIS RR data have approximately the same 1 km spatial resolution as the full-resolution SeaWiFS and MODISA data. OCTS, SeaWiFS and MODISA Level-2 data (i.e. processed to surface quantities but unmapped) were obtained from NASA's Ocean Color website (http://oceancolor.gsfc.nasa.gov/) and MERIS Level-2 data were obtained from ESA's MERIS Catalog and Inventory (http://merci-srv.eo.esa.int/merci/welcome.do).

For each Level-2 pixel we used the corresponding Level-2 flags. A pixel was determined valid if none of the following flags were set: ATMFAIL, LAND, HISATZEN, CLDICE, CHLFAIL, SEAICE, NAVFAIL, HIPOL and PRODFAIL. Standard ESA MERIS processing use different flags. If any of the following MERIS flags was set then the pixel was considered invalid: LOW SUN, HIGH_GLINT, ICE_HAZE, SUSPECT, COASTLINE, PCD_19, PCD_18, PCD_17, PCD_16, PCD_15, PCD_14, PCD_1_13, CLOUD and LAND.

The use of 3×3 pixel statistics instead of the single value gives an estimate of the statistical variability in the neighborhood of the in situ sample and allows for screening of satellite pixels according to pixel to pixel variability, closeness to cloud edges, etc. Satellite pixels close to cloud edges have increased errors in the derived variables and were removed from the match-up dataset.

For each 3×3 pixel area we calculated the following statistical parameters: number of valid pixels (*nValid*), minimum (*SatMin*), maximum (*SatMax*), arithmetic mean (*Csat*), median and standard deviation. We first found gross match-ups defined as those within 5 days of the in situ sample and with at least 3 valid pixels out of the 9 possible. We then used the following screening criteria to refine the match-ups, keeping only the most accurate and representative match-ups and eliminating the more questionable or lower quality match-ups:

(1) time difference with in situ sample < 12 h.
(2) $(SatMax - SatMin)/Satmin < 1$.
(3) $nValid \geq 7$.

It turned out that at high in situ *Chl-a* levels very few refined match-ups were obtained if requiring 7 or more valid pixels. Therefore, the last condition was relaxed to $nValid \geq 3$ if $Cins \geq 2$. In the statistics we used the mean of the valid match-up pixels, *Csat*.

We also counted the outliers from the mean relationships by using the ratio of the mean satellite value (*Csat*) to the in situ value (*Cins*). The match-ups with $Csat/Cins > 3$ and those with $Csat/Cins < 1/5$ were defined as outliers. As a result, we obtained

Table 1
Annual distribution of high-quality surface *Chl-a* stations.

Year	No. of stations
1996	392
1997	544
1998	714
1999	543
2000	518
2001	642
2002	750
2003	922
2004	557
2005	638
2006	725
2007	670
2008	1224
2009	909
2010	302
Total	10,050

14,260 gross and 2322 refined match-ups with all four sensors (Fig. 1, Table 2). The MERIS *Algal_2* product had high scatter and significant bias and was excluded from further analysis. The MERIS *Algal_1* product (Morel and Antoine, 2007) was therefore used as the MERIS *Chl-a* estimate.

While all satellite sensors showed quite similar positive correlations with in situ data (Fig. 2) with the coefficient of determination (r^2) for the refined match-ups ranging from 0.791 (SeaWiFS) to 0.864 (OCTS), they also showed slight over-estimation at low *Cins* and significant under-estimation at high *Cins*. The Root Mean Square error (RMS) calculated for log 10-transformed data was highest for OCTS and quite similar for the other three sensors. Satellite estimates of *Chl-a* corresponding to *Cins* higher than $\sim 1\ mg\ m^{-3}$ significantly underestimated in situ *Chl-a*, especially for OCTS, SeaWiFS and MODIS. All outliers with *Csat*/*Cins* < 1/5 were within the nearshore band extending ~100 km from the coast. It is difficult to separate bio-optical effects related to coastal waters from the effect of high *Chl-a* as high *Chl-a* levels occur almost exclusively in the coastal areas. The problem of missing high *Csat* for corresponding high *Cins* values (highlighted by the empty circles in Fig. 2) was worse for MODISA than for other sensors. For MODISA less than 3% (1 out of 35) of the refined match-ups with $Cins > 2\ mg\ m^{-3}$ had a matching $Csat > 2\ mg\ m^{-3}$. For SeaWiFS 14% (23 out of 164) of the refined match-ups with $Cins > 2\ mg\ m^{-3}$ had the corresponding $Csat > 2\ mg\ m^{-3}$. MERIS was least affected by the underestimation at high *Chl-a* with 70% (64 out of 92) of $Cins > 2\ mg\ m^{-3}$ with the corresponding $Csat > 2\ mg\ m^{-3}$. The MERIS regression statistics were improved by the four refined match-ups with very high *Chl-a* ($> 10\ mg\ m^{-3}$) in both *Cins* and *Csat* (Fig. 2). The strong effect of a few match-up points highlights a general problem: in spite of the large number of in situ data and the large number of high-quality match-ups, their uneven distribution in the full *Chl-a* range makes it difficult to create a reliable statistical fit through the full range of *Chl-a*. This is especially evident at $Cins > 10\ mg\ m^{-3}$ where both the small number of matchups and their large scatter makes it difficult to constrain the statistical relationships between *Chl-a* and bio-optical properties.

Standard ocean color algorithms for *Chl-a* use empirical models between log 10-transformed *Cins* and log 10-transformed maximum band ratio (*MBR*) of remote sensing radiance (*Rrs*) (O'Reilly et al., 1998, 2000). *MBR* is calculated as the maximum of *Rrs* at several wavelengths (e.g. *Rrs443*, *Rrs490*, *Rrs510* for SeaWiFS) to the *Rrs* of the green band (e.g. *Rrs555* for SeaWiFS). The current NASA operational *Chl-a* algorithm is OC4v6 with slightly different versions for each sensor (http://oceancolor.gsfc.nasa.gov/REPROCESSING/R2009/ocv6/). The scatter of gross and

Table 2
Number of *gross* and *refined* match-ups for different satellite sensors.

Sensor	Gross	Refined
OCTS	257	66
SeaWiFS	6542	1075
MODISA	4018	650
MERIS	3443	531
All	14,260	2322

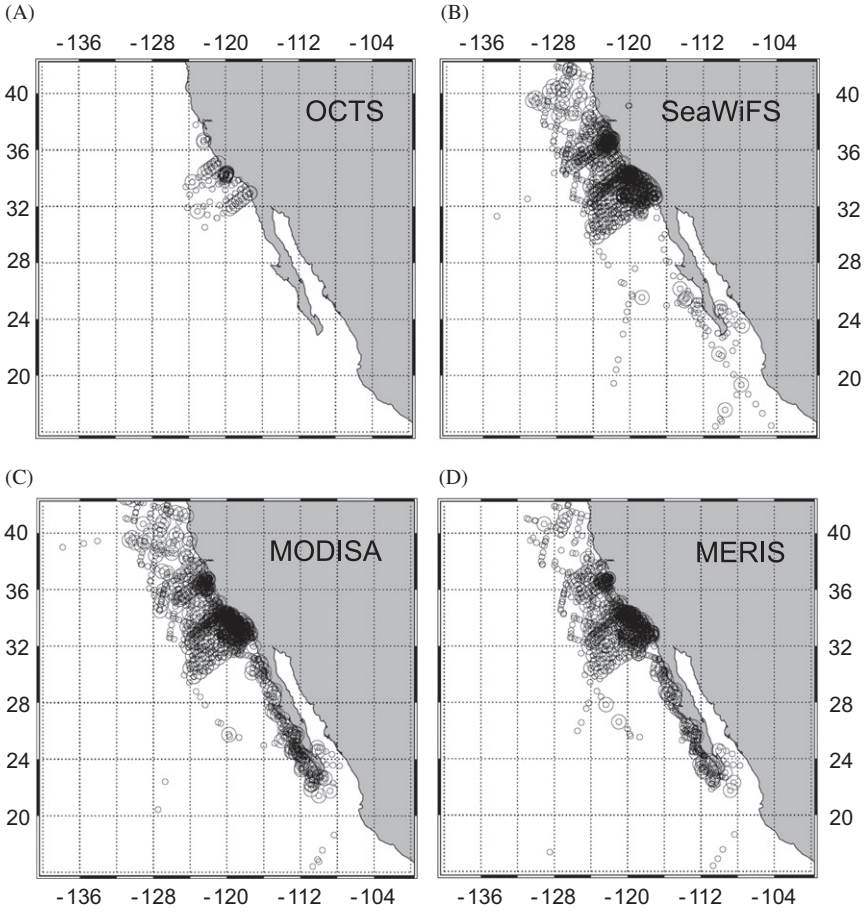

Fig. 1. Locations of the gross (small circles) and the refined (bigger circles) match-ups for OCTS, SeaWiFS, MODISA and MERIS.

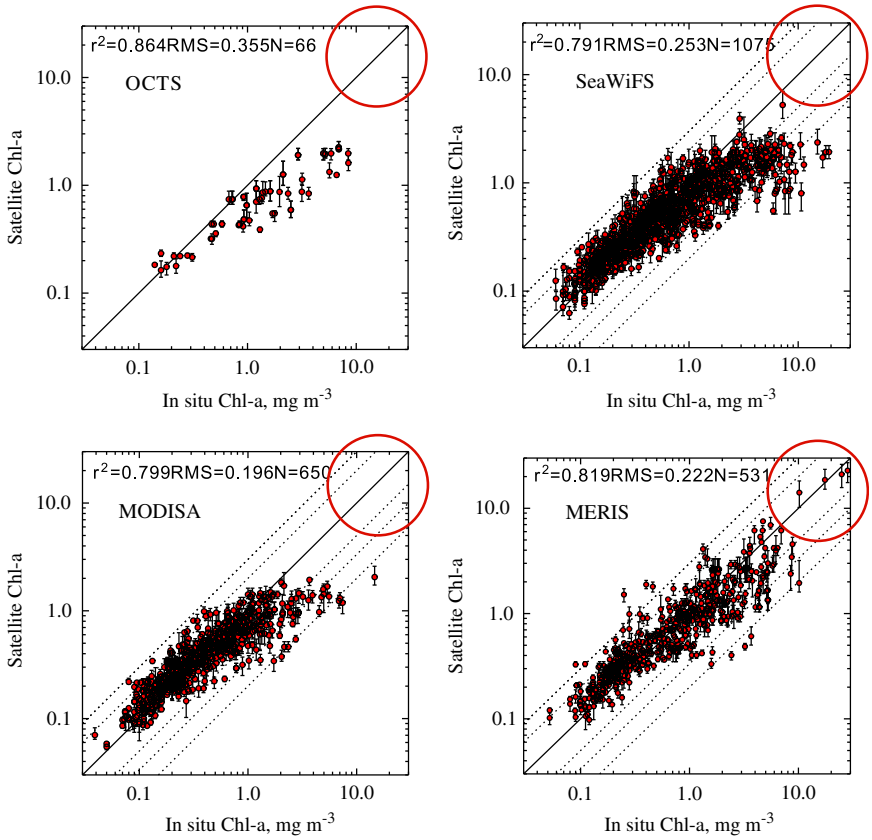

Fig. 2. Refined match-ups between in situ *Chl-a* values and satellite-detected *Csat* for OCTS, SeaWiFS, MODISA and MERIS. The red circles highlight the regions of missing match-ups at high *Chl-a* except for MERIS. The vertical lines associated with each point show the minimum and maximum values in the 3×3 pixel match-up window. The dotted lines above the one-to-one (solid) line show *Csat* overestimation of in situ values by, respectively, 2 and 3 times. The dotted lines below the one-to-one line show *Csat* underestimation by 2, 3 and 5 times. (For interpretation of the references to color in this figure legend, the reader is referred to the web version of this article.)

refined match-up points shows a significant deviation from the standard algorithms, especially at high *Cins* (Fig. 3). The distribution of match-up points over the full range of *Chl-a* is extremely uneven: there are many points in the middle range and few points at both ends. In order to reduce the effect of the uneven distribution of match-up points we followed Gregg et al. (2009) and aggregated the refined match-ups into small brackets by using median values of log 10(*Cins*) and the medians of the corresponding log 10(*MBR*). As a result, we reduced the effects of the uneven distribution of match-up points and the effect of random errors (Fig. 4). These derived points are called "bracket" points. With the exception of OCTS that had too few match-ups, the bracket points of all the sensors show relatively smooth distributions that are better suited for developing statistical models than the original match-ups. We then fitted 4-th order polynomials as used by the standard OC4/OC3 models to the log 10-transformed *Cins* versus *MBR* bracket points for each sensor. The results show systematic deviations from the standard OC3/OC4 algorithms (Fig. 4). Considering the logarithmic scale of these plots, the differences with the standard algorithms are quite large and need to be eliminated in order to reduce the bias in satellite-detected *Chl-a*. For OCTS we do not have match-ups for $Cins < 0.16$ mg m^{-3} ($MBR > 4.52$) and cannot constrain the fitted curve in the low *Chl-a* range. We therefore use the standard OC4Ov6 algorithm at $MBR > 4.52$.

2.3. Optimizing the ocean color algorithms for multiple sensors using in situ data

In order to create the best algorithms for multiple sensors that are consistent with both in situ data as well as with each other, we have 2 tasks: (1) minimize the RMS bias with in situ data; and (2) minimize the difference between the products of different sensors. Ideally, with adequate number of match-up points distributed uniformly over the full range of possible values, task 2 would automatically follow from task 1. However, as shown in previous sections, even with the total number of in situ samples over 10,000 and hundreds of refined match-ups (over 1000 for SeaWiFS), the distribution of match-up points is highly non-uniform and, most importantly, is missing sufficient number of match-up points at high *Cins*. Moreover, the distribution of match-up points is biased not just along the *Chl-a* value axis but also in terms of other criteria, such as distance from coast, location along the north–south and/or east–west axes (Fig. 1), time of the year, etc. Therefore, using algorithms derived solely from minimizing the difference with a limited and non-uniformly distributed set of in situ data (task 1) lead to systematic differences between the products of different sensors. The statistical differences between the different sensors actually increased for the best-fit algorithms compared to the standard algorithms. The increase for between-sensor differences was partially caused by the increased *Chl-a* estimates at low MBR using poorly constrained model fits. We therefore need to perform the additional task 2 to minimize the differences between different sensors while not letting the results deviate too much from the relationships obtained in task 1.

For our task 2 we used daily Level-3 satellite data for each sensor and created a matching dataset of *MBR* values for the temporally overlapping sensors (SeaWiFS, MODISA and MERIS). SeaWiFS and MODISA Level-3 datasets were downloaded from NASA's Ocean Color website (http://oceancolor.gsfc.nasa.gov/) and MERIS Level-3 data were obtained from ESA's Earthnet Online

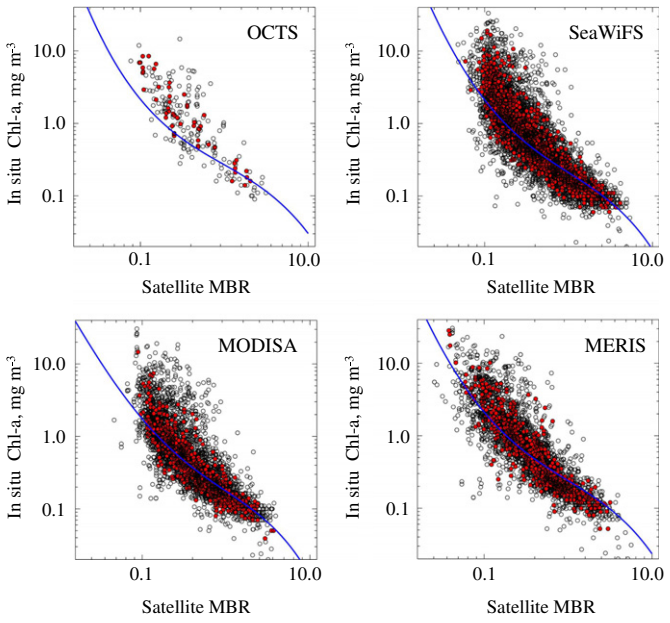

Fig. 3. Scatter plots of the gross (black circles) and refined (red circles) match-ups of in situ *Chl-a* versus the satellite estimated maximum band ratio (*MBR*) of remote sensing reflectances for OCTS, SeaWiFS, MODISA and MERIS. Blue curves show the respective standard OC4/OC3 algorithms. (For interpretation of the references to color in this figure legend, the reader is referred to the web version of this article.)

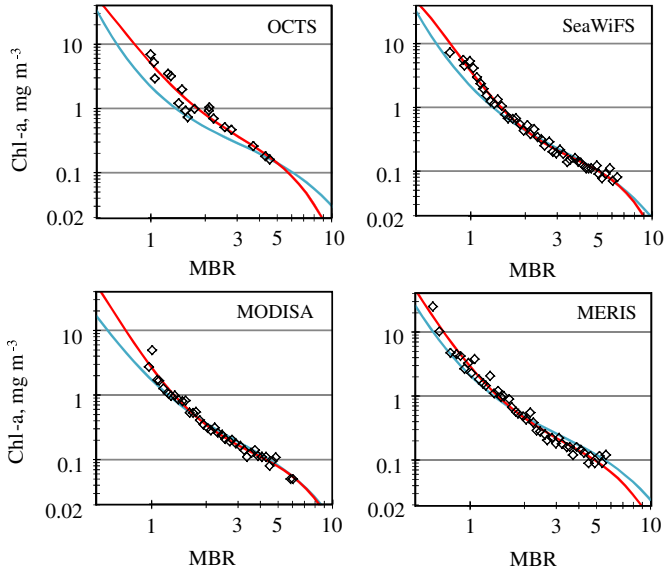

Fig. 4. Scatter plots of the median match-ups ("brackets") of in situ *Chl-a* versus satellite estimated maximum band ratio (*MBR*) for OCTS, SeaWiFS, MODISA and MERIS. The standard OC3/OC4 algorithms (blue curves) and the best fits to the bracket points (red curves) are shown. (For interpretation of the references to color in this figure legend, the reader is referred to the web version of this article.)

(http://earth.eo.esa.int). Daily mean *Rrs* values were calculated for different sensors over a grid of 1° latitude × 1° longitude covering approximately 1000 km wide area from northern California to the southern tip of the Baja California peninsula (Fig. 5). Those daily mean *Rrs* values of different sensors were then matched with each other, keeping only those matching *MBR* values with at least 66% of the pixels within each 1° × 1° sub-area having valid values. The last requirement eliminated a large number of daily *MBR* data which missed more than 1/3 of the pixels due to clouds or orbit differences. As a result, a total of 7467 matching *MBR* values for

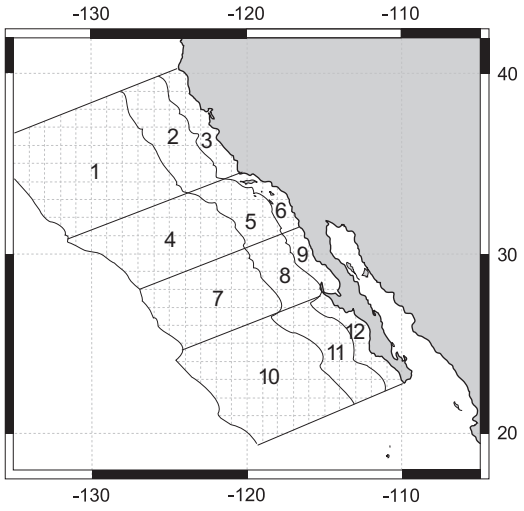

Fig. 5. Grid of 1° latitude × 1° longitude (thin dashed lines) areas from northern California to the southern tip of Baja California and a grid of 12 large areas parallel and across the mean coastline. The bands parallel to coastlines are coastal (0–100 km), transition (100–300 km) and offshore (300–1000 km). The north–south bands are called Central California, Southern California, Northern Baja California and Southern Baja California, respectively.

all three sensors were found. We then used a complex optimization procedure to minimize the deviations between the calculated *Csat* and *Cins* of the bracket points and the absolute differences in *Csat* between the three sensors over the matching 1° × 1° sub-areas. When using all the 7467 matching *MBR* values with the much smaller number of bracket points the minimization process would be dominated by the matching *MBR* values at the expense of the *Csat* and *Cins* comparison. Without giving the *Csat*/*Cins* comparison more weight the minimization of the absolute differences in *Csat* between the sensors would tend to create models that result in low and nearly constant *Csat* values. To balance these constraints, we performed the optimization by using an equal number of *Csat*/*Cins* comparisons on one hand and the between-sensor *Csat* comparisons on the other. For the *Csat*/*Cins* comparison we used a set of 134 bracket points of all three temporally overlapping sensors (47 for SeaWiFS, 40 for MODISA and 47 for MERIS). For the between-sensor *Csat* comparison we picked the same number (134) matching *MBR* points. We selected those points by first sorting all matching sensor-to-sensor match-ups by the *Csat* value and then picked half of the points from the bottom of the range and the other half of the points from the top of the range. The coefficients of the 4-th order polynomials obtained from fitting the *Cins*/*MBR* brackets for each sensor (corresponding to the red curves in Fig. 4) were used as the starting points of the minimization process which optimizes the 15 coefficients (5 for each sensor) of the three overlapping sensors. For the optimization we used the Trust-Region method, a variant of the Levenberg–Marquardt method as implemented in the NMath 5.0 numerical libraries (http://www.centerspace.net/). The resulting sets of optimized coefficients (called CALFIT) are shown in Table 3. For OCTS the final algorithm has 2 branches: a fit to the *MBR-Cins* brackets for $MBR \leq 4.52$ and the standard NASA OC4Ov6 algorithm for $MBR > 4.52$.

2.4. Statistical estimates of model robustness

Following optimization, we performed statistical comparison between the three temporally overlapping sensors. We used several statistical measures to evaluate the performance of the different algorithms. Absolute Bias (AbsBias in Table 4) was calculated as the median of the absolute percent error of the

three sensors for all the overlapping $1^\circ \times 1^\circ$ regions. Absolute percent error for each of the overlapping small areas was defined as the sum of absolute deviations from the mean (of the 3 sensors) divided by the number of sensors (3), then divided by the mean and multiplied by 100. The mean absolute percent difference between the 3 sensors was calculated for the *Csat* values (AbsDiff% in Table 4) and a similar measure, mean absolute error (AbsDiffLog in Table 4) for the for log 10-transformed *Csat* data.

The Semi-Interquartile Range (SIQR) was calculated for the distribution of the absolute percent error of the three sensors and provides an estimate of the spread or dispersion of the data. SIQR is analogous to the standard deviation for normally distributed data but is a more robust estimate for skewed data as it is not strongly affected by outliers. In contrast to AbsBias and SIQR, another measure of scatter, the Root Mean Square error (RMS) was calculated on log 10-transformed estimates of *Csat*. Both AbsBias and SIQR are based on ratios to the mean and do not need to be performed on log-transformed data. We also calculated the slope of a linear regression between log 10-transformed *Csat* values of one sensor versus log 10-transformed *Csat* values of another sensor.

3. Results

3.1. Algorithm comparison

A comparison of the results of applying the standard NASA/ESA algorithms, the fit to the brackets of *Csat*/*Cins* and the optimized algorithms (CALFIT) as applied to the 7467 matching MBR values in $1^\circ \times 1^\circ$ grid of the California Current region are shown in Table 4 and Fig. 6. The optimized CALFIT algorithms showed improvement in making the slopes of the sensor-to-sensor comparison closer to unity, e.g. from 0.962 to 1.02 for MODISA versus SeaWiFS and from 0.822 to 0.893 for MERIS versus SeaWiFS. More importantly, they increased the higher *Csat* values that were much too low in the *Csat*/*Cins* comparisons in Fig. 2. However, at the same time CALFIT also increased the scatter around the one-to-one line and the estimates of variance. The standard NASA OC4/OC3 version 6 algorithms (http://oceancolor.gsfc.nasa.gov/REPROCESSING/R2009/ocv6/) produce good agreement between SeaWiFS and MODISA with MODISA slightly higher at the lowest *Csat* values but in the comparison with *Cins* they both significantly underestimate *Cins* at the higher *Cins* values. The under-estimation at *Cins* > 1 is often 5 times or more (Fig. 2) and may cause significant bias in the coastal zone. CALFIT improves the MERIS versus SeaWiFS comparison by making the slope closer to one. It is obvious that using the coefficients obtained by fitting the *Csat* data to *Cins* data alone (the "Fit to Brackets" row in Table 4) is not the best option as it actually increases the between-sensor difference and the estimates of variance due to the increased values and scatter at higher *Csat* levels. It appears that the requirements of minimizing the *Csat*/*Cins* differences on one hand and minimizing the between-sensor *Csat* differences on the other are not totally compatible with each other and do not allow the slope of the MERIS versus SeaWiFS *Csat* to be closer to one. This is probably caused by the statistically not representative sets of match-ups at high *Cins*. To summarize, the optimized CALFIT algorithms are not perfect but represent a significant improvement compared to both the NASA/ESA standard algorithms and to the algorithms created by fitting satellite *Rrs* data to the match-up *Cins* data.

For OCTS we did not have any temporally overlapping *MBR* data from other satellite sensors and therefore we were limited to use only the fit to the brackets of in situ match-ups. At high *MBR* values the CALFIT algorithm for OCTS switches to the standard OC4Ov6 algorithm. Although we cannot directly compare the results of OCTS to another temporally overlapping sensor, the significantly improved fit to the match-up brackets compared to the standard NASA algorithm justifies the use of a new algorithm.

Table 3
CALFIT optimized 4th order polynomial coefficients of the OC4/OC3 type models for calculating *Csat* from the maximum band ratio (*MBR*) of remote sensing radiances for different satellite sensors. The relationship with $R = \log 10(MBR)$ is: $\log(Csat) = a_0 + a_1R + a_2R^2 + a_3R^3 + a_4R^4$. For OCTS the algorithm switches to the standard NASA OC4Ov6 algorithm (OCTS*) for $MBR > 4.52$.

	a_0	a_1	a_2	a_3	a_4
OCTS	0.6929	−3.1722	1.5019	1.7696	−2.7999
OCTS*	0.3325	−2.8278	3.0939	−2.0917	−0.0257
SeaWiFS	0.4743	−3.4300	1.2953	3.7343	−3.8935
MODISA	0.3972	−3.7832	2.5636	1.8097	−3.0309
MERIS	0.4975	−3.4758	2.3330	0.8054	−1.8828

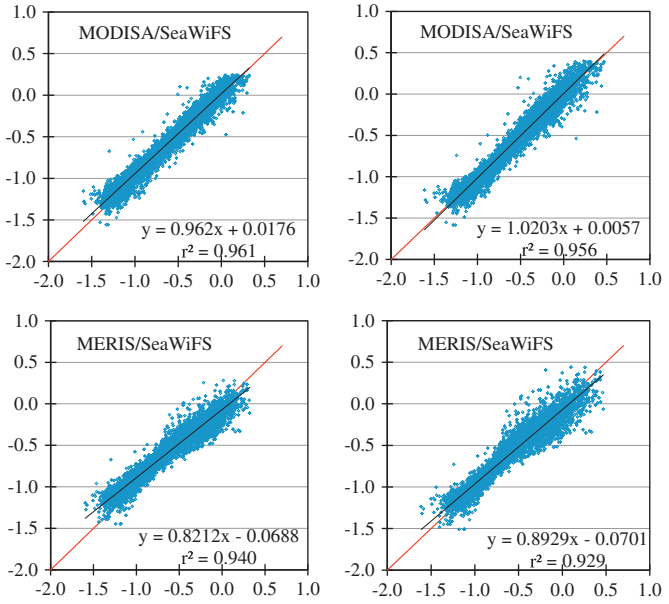

Fig. 6. Scatter plots of log 10-transformed satellite estimates of *Chl-a* (*Csat*) between MODISA and SeaWiFS (top panels) and between MERIS and SeaWiFS (bottom panels) using the standard OC3/OC4 version 6 algorithms (left panels) and the optimized CALFIT versions (right panels). Red line is the one-to-one line and black line is the regression line. (For interpretation of the references to color in this figure legend, the reader is referred to the web version of this article.)

Table 4
Comparison of the application of the three algorithms on the matching 4467 sub-areas of $1^\circ \times 1^\circ$ in the California Current. See Section 2.4 for explanations.

	AbsBias	AbsDiff%	AbsDiffLog	SIQR	RMS	Slope log MOD/log SWF	Slope log MERIS/log SWF
Standard OC4/OC3	9.796	11.24	0.0495	3.762	0.116	0.962	0.821
Fit to brackets	8.744	11.70	0.0527	4.877	0.139	0.962	0.858
Optimized for brackets and *MBR*	7.951	10.57	0.0468	4.208	0.124	1.020	0.893

3.2. Time series of the merged multi-sensor Csat

We applied the CALFIT algorithms (Table 3) to the daily Level-3 datasets of *Rrs* of the four sensors (OCTS, SeaWiFS, MODISA and MERIS). Merged daily CALFIT *Chl-a* datasets were composited as means of the valid individual sensor values. The merged daily CALFIT *Chl-a* datasets were then composited into monthly datasets. In order to examine various time series in different regions of the California Current we used a grid of 3 by 4 areas (Fig. 5) from offshore (approximate distance from coast 300–1000 km) through transition zone (100–300 km from coast) to coastal zone (0–100 km from coast), and from north to south as Central California (areas 1–3), Southern California (areas 4–6), Northern Baja California (areas 7–9) and Southern Baja California (areas 9–12). This grid has been used in the past (e.g. Kahru and Mitchell, 2001) and derives from the work of Lynn and Simpson (1987) who showed that the variability structure of dynamic height in the California Current can be divided into offshore, transition and coastal bands that are roughly parallel to the coast. For each of the 12 areas we created time series using the monthly CALFIT *Chl-a* datasets and the means of each area were plotted. In addition to the strong annual cycle, the offshore areas (Fig. 7, area 1) seem to have a periodic pattern with two approximately 8-year periods (1997–2004, 2005–2012). Some of the coastal and transition areas seem to show a trend of increasing annual maxima (Fig. 7, area 6). The annual cycle is clearly dominating the overall variability in *Csat*. In order to remove the effects of the annual cycle we calculated monthly anomalies by first calculating the average monthly *Csat* value for each pixel and then using the ratio of monthly values to the mean value of the respective month. The ratio anomaly was expressed as percentage anomaly with $100 \times (\text{Anomaly} - 1)$. Anomaly plots show no significant trend in some areas (Fig. 8, area 1), a significant ($P < 0.01$) trend of increasing *Csat* in some of the coastal and transition areas (Fig. 8, area 3), and significant ($P < 0.01$) trend of decreasing *Csat* in the southern offshore areas (Fig. 8, area 10).

To get a more detailed spatial distribution of the potential trends we evaluated the trends and their significance for each of the $9\,\text{km} \times 9\,\text{km}$ pixels using the nonparametric Sen slope estimator (Sen, 1968; Gilbert, 1987). The nonparametric Mann–Kendall test was used to evaluate the statistical significance of the trend according to Salmi et al. (2002). Significant trends (at 95% confidence level) of increasing *Csat* in the coastal and transition zones of Central and Southern California and decreasing *Csat* in the transition and offshore areas of the Southern Baja areas were detected (Fig. 9). Although we have not validated the CALFIT algorithm for the North Pacific Gyre outside the California Current

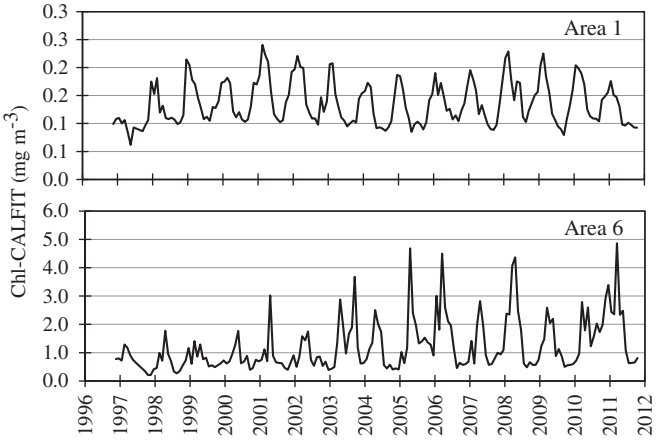

Fig. 7. Time series of the merged multi-sensor (OCTS, SeaWiFS, MODISA, MERIS) *Chl-a* for area 1 (offshore Central California) and area 6 (coastal Southern California) of the California Current grid (Fig. 5).

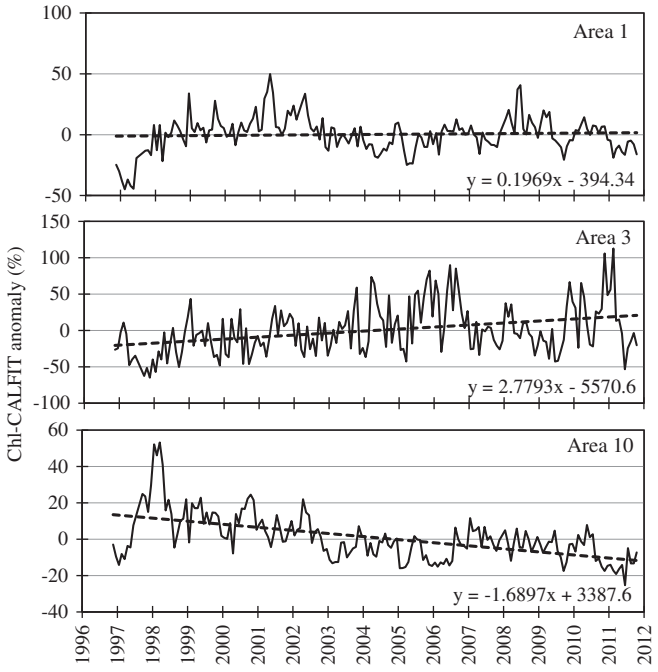

Fig. 8. Time series of the anomaly of the merged multi-sensor (OCTS, SeaWiFS, MODISA, MERIS) *Chl-a* for areas 1, 3 and 10 of the California Current grid (Fig. 5). The anomaly is a ratio of the current month value to the mean value of the particular month. The trends in areas 3 and 10 are significant ($P < 0.01$).

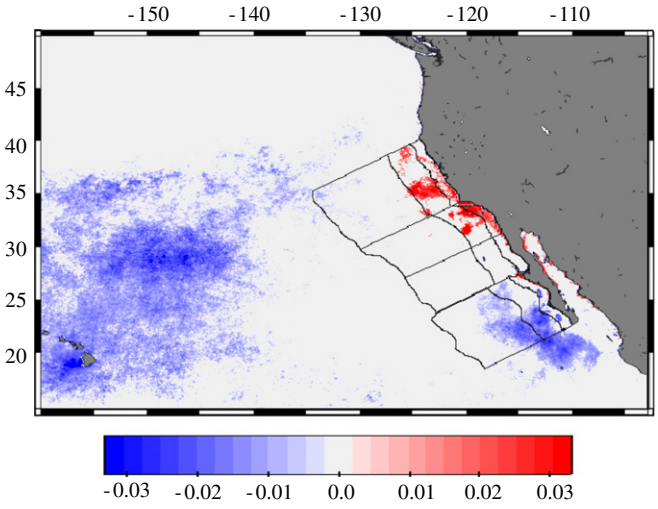

Fig. 9. Estimated trends in the multi-sensor (OCTS, SeaWiFS, MODISA, MERIS) merged *Chl-a* (1996–2011). The grid of 12 selected areas in the California Current is overlaid. Estimated trends below the 95% confidence level are shown in white.

we extended the evaluated area west to the Hawaiian Islands. The observed pattern of a significant decreasing trend in *Chl-a* anomalies is clearly visible in the North Pacific gyre waters and is consistent with the earlier reports on "expanding ocean deserts" (Behrenfeld at al., 2006; Polovina et al., 2008).

4. Discussion

Merging data from multiple sensors is needed to both extend the time series from a limited time period available from a single sensor and to improve the coverage and decrease the sampling errors (IOCCG, 2007). Compared to data from individual sensors, the merged

products from three ocean color sensors have approximately twice the mean global coverage and lower uncertainties in the retrieved variables (Maritorena et al., 2010). GlobColour project of the European Space Agency is using multiple methods to merge water-leaving radiances or *Chl-a* from three sensors (SeaWiFS, MERIS, and MODISA) (Maritorena et al., 2010). While systematic differences exist between the products of individual sensors, the large scale *Chl-a* distributions produced by the major ocean color missions are consistent over a wide range of conditions (Morel et al., 2007; Djavidnia et al., 2010). However, these methods typically do not include in situ data in the data merger process and may produce large differences from in situ data. Gregg and Conkright (2001) pioneered the blending of satellite *Chl-a* data with in situ data and Gregg et al. (2009) introduced a method they called the Empirical Satellite Radiance-In situ Data (ESRID). Using ESRID Gregg and Casey (2010) were able to drastically reduce the discrepancy between global *Csat* retrievals of SeaWiFS and MODISA. We followed the ideas of ESRID with some important modifications. First, we used high-resolution Level-2 data instead of the 9×9 km Level-3 satellite data for comparison with in situ data as match-ups. Match-ups with low-resolution satellite data may introduce systematic errors, particularly in regions of high spatial variance such as the coastal waters of the California Current System. *Csat* calculated from 9-km Level-3 data is averaged over a large area ($\sim$100 km^2) that is likely to smooth the small-scale high values lower and small-scale low values higher, thus creating a systematic bias in the *Csat*/*Cins* comparison. Instead, we used satellite data with the highest routinely available spatial resolution for match-ups. Even at 1-km spatial resolution we see large discrepancies, especially at high *Cins* (Fig. 2), some of which is due to sub-pixel variability of satellite data that is especially relevant at high *Chl-a* in the coastal zone. We observed that an optimization using the median brackets of satellite *MBR* and *Cins* will not produce compatible *Csat* values between multiple sensors due to the poorly constrained variance between high *Cins* and *MBR*. As another modification to ESRID, we added the second step of minimizing the deviations of both the *MBR* and *Cins* pairs as well as the between-sensor differences at a set of selected points of *MBR*. Due to these modifications we call our method Local Empirical Satellite Radiance-in situ Data or LESRID. As our approach is applied regionally to the California Current, the CALFIT coefficients may not be ideal for other regions but the approach can be applied to other regions with available in situ data. It is possible that the CALFIT algorithms (coefficients in Table 3) are applicable to other bio-optically simple (Case 1) regions of the world ocean. Compared to the application of ESRID by Gregg and Casey (2010), our application of LESRID did not result in such a dramatic reduction of between-sensor discrepancies. This is explained by the following facts: (1) we used the latest NASA reprocessed data that already had drastically reduced differences between SeaWiFS and MODISA; (2) major differences between sensors and with in situ data were not in the open ocean with low *Chl-a* and low variability but in coastal waters with highest *Chl-a*, highest natural bio-optical variability and fewest reliable match-ups; (3) we included MERIS which is being processed by ESA with methods that are different from the methods used by NASA Ocean Color Processing Group for SeaWiFS and MODISA data.

It appears that the current standard NASA algorithms for SeaWiFS and MODISA underestimate *Chl-a* significantly in the coastal zone at *Chl-a* > 1. The LESRID procedure introduced here improved the compliance with in situ data and at the same time reduced the differences in retrievals between different sensors. However, our current simplistic models will not lead to perfect agreement between sensors. As noted by others (Morel et al., 2007; Gregg and Casey, 2010), different sensors not only observe chlorophyll distributions differently but also observe different chlorophyll distributions. In order to improve the algorithms in the coastal zone we need to collect much more *Chl-a* and other bio-optical data in the highly variable coastal zone, produce better models that explain the divergent bio-optical properties at high *Chl-a* where concentrations of chlorophyll and potentially non-covarying optical constituents (e.g. colored dissolved material and suspended solids) are high and the complexities in both the atmospheric correction and in the bio-optical algorithms are the highest. While the resulting merged time series of *Csat* in the California Current is not perfect, it is a step forward towards creating unified climate data records that are needed to evaluate climate-related trends using data merged from multiple and different sensors.

By using the unified time series of merged ocean color satellite data we were able to show significant changes in the California Current during the last 15 years (1996–2011). We detected significant increase in surface *Chl-a* in the coastal and transition zones of Central California and significant decrease off Southern Baja California. We also confirmed the existence of the previously noted decrease of *Chl-a* in the Northern Pacific Gyre, the so-called expansion of ocean deserts (Polovina et al., 2008). The trend of increasing *Chl-a* off Central California is consistent with the observed increase in upwelling-favorable winds and wind-driven coastal upwelling during the period of 1982–2008 (García-Reyes and Largier, 2010). Increased upwelling off central California has been predicted and is assumed to be the result of increased onshore–offshore atmospheric pressure gradients and enhanced alongshore winds due to global warming (Bakun, 1990; Di Lorenzo et al., 2005; Auad et al., 2006). Another interesting result on future trends, produced from model analysis (Rykaczewski and Dunne, 2010), projects increases in nitrate supply and productivity in the CCE during the 21st century despite increases in stratification and limited change in wind-driven upwelling due to increased nitrate supply in the deep source waters entering the CCE resulting from decreased ventilation of the North Pacific.

Although this 15-year time series is too short to separate interannual and multidecadal cycles from climate trends (Henson et al., 2010), both of the observed trends are consistent with the predicted effects of climate change: lower productivity in the gyres due to stronger stratification and weaker vertical nutrient fluxes and higher productivity in the central California upwelling zone either due to increased upwelling or increased nitrate concentration in the upwelled waters. The explanation for the decrease of *Chl-a* off Southern Baja remains elusive but the pattern looks similar to the area where *Chl-a* was increased during the 1997–98 and 1982–83 El Niños (Kahru and Mitchell, 2000). Thus this pattern may be indicative of weaker El Niño events, corresponding to a weakening of the positive anomalies seen during El Ninos. The 1998 *Chl-a* maximum (Fig. 8, area 10) in the beginning of the time series certainly contributed to the overall decreasing trend but a decreasing trend is still evident after 1998.

5. Conclusions

We created algorithms for four ocean color sensors (OCTS, SeaWiFS, MODISA, MERIS) that are empirically tuned to a large archive of in situ *Chl-a* data and also consistent between the different sensors. This analysis is an important first step towards creating Climate Data Records for coastal waters such as the southern California Current System. While there is clearly still room for improvement, the merged, 15-year record demonstrates that there are multi-decadal trends in chlorophyll that are not simply artifacts of sensor design or processing methodology. Using these algorithms we created a consistent multi-sensor time series of the surface *Chl-a* concentration in California Current region. The merged *Chl-a* time series (November 1996–October 2011) shows a significant trend of increasing *Chl-a* off central California, consistent with increased upwelling or increased

Table A1
List of symbols.

Symbol	Explanation	Units
Chl-a	Chlorophyll-a concentration	$mg\,m^{-3}$
Cins	Surface in situ Chl-a value	$mg\,m^{-3}$
Csat	Satellite Chl-a estimate	$mg\,m^{-3}$
MBR	Maximum band ratio of *Rrs*	
nValid	Number of valid pixels in 3×3 pixel window	
r	Correlation coefficient	
Rrs	Remote sensing reflectance	sr^{-1}
Rrs443	Remote sensing reflectance at 443 nm	sr^{-1}
Rrs490	Remote sensing reflectance at 490 nm	sr^{-1}
Rrs510	Remote sensing reflectance at 510 nm	sr^{-1}
Rrs555	Remote sensing reflectance at 555 nm	sr^{-1}
SatMin	Minimum pixel value in 3×3 pixel window	$mg\,m^{-3}$
SatMax	Maximum pixel value in 3×3 pixel window	$mg\,m^{-3}$

Table A2
List of acronyms.

Acronym	Explanation
CalCOFI	California Cooperative Oceanic Fisheries Investigations
CALFIT	Name of the *Chl-a* algorithms developed in this work
CCE-LTER	California Current Ecosystem Long Term Ecological Research
Delphinus	NOAA SWFSC survey of *Delphinus* species (Chivers et al., 2010)
ESRID	Empirical Satellite-In situ Data (Gregg et al., 2009)
Line 60	CalCOFI Line 60 occupied by Monterey Bay Aquarium Research Institute
Line 67	CalCOFI Line 67 occupied by Monterey Bay Aquarium Research Institute
MERIS	Medium resolution imaging instrument on ESA Envisat satellite
MODISA	Moderate Resolution Imaging Spectroradiometer on NASA Aqua satellite
MODIST	Moderate Resolution Imaging Spectroradiometer on NASA Terra satellite
OC3	Ocean Color algorithm using 3 bands (O'Reilly et al., 1998)
OC4	Ocean Color algorithm using 4 bands (O'Reilly et al., 1998)
OC4v6	Ocean Color algorithm using 4 bands, version 6
OC4Ov6	Ocean Color algorithm using 4 bands for OCTS, version 6
OCTS	Ocean Color and Temperature Sensor on Japan ADEOS satellite
Orcawale	NOAA SWFSC survey of whales, dolphins, and porpoises, 2008
PACOOS	Pacific Coastal Ocean Observing System
SeaBASS	NASA Bio-optical Archive and Storage System with the investigator's name
SeaWiFS	Sea-viewing Wide Field-of-view Sensor

Table A3
Total number of surface *Chl-a* stations used. The acronyms of the projects are listed in Table A2.

Data source, PI	1996–2010
CalCOFI	4341
CCE-LTER	818
Orcawale	405
SeaBASS, Arnone	83
SeaBASS, Chavez	537
Line 60	123
Line 67	556
SeaBASS, Mitchell	101
SeaBASS, Nelson	4
Delphinus	465
SeaBASS, Siegel	2132
SeaBASS, Stramski	45
SeaBASS, Stumpf	23
SeaBASS, Trees	66
SeaBASS, Zettler	83
CCE-LTER, HPLC	34
CCE-LTER, Chekalyuk	115
PACOOS	119
Total	10,050

nutrient input, and a trend of decreasing *Chl-a* off southern Baja California.

Acknowledgments

Financial support was provided by the NASA Ocean Biology and Biogeochemistry Program, the University of California Institute for Mexico and the United States (UC MEXUS) and Consejo Nacional de Ciencia y Tecnología, Mexico (CONACYT). Satellite data were provided by the NASA Ocean Color Processing Group and ESA MERIS team. We thank the many research programs that made in situ chlorophyll data available for this analysis.

Appendix A

See Table A1–A3.

References

Aksnes, D.L., Ohman, M.D., 2009. Multi-decadal shoaling of the euphotic zone in the southern sector of the California Current System. Limnol. Oceanogr. 54, 1272–1281.
Antoine, D., d'Ortenzio, F., Hooker, S.B., Bécu, G., Gentili, B., Tailliez, D., Scott, A.J., 2008. Assessment of uncertainty in the ocean reflectance determined by three satellite ocean color sensors (MERIS, SeaWiFS and MODIS-A) at an offshore site in the Mediterranean Sea (BOUSSOLE project). J. Geophys. Res. 113, C07013.
Auad, G., Miller, A., Di Lorenzo, E., 2006. Long-term forecast of oceanic conditions off California and their biological implications. J. Geophys. Res. 111, C09008, http://dx.doi.org/10.1029/2005JC003219.
Bailey, S., Werdell, P., 2006. A multi-sensor approach for the on-orbit validation of ocean color satellite data products. Remote Sensing Environ. 102, 12–23.
Bakun, A., 1990. Global climate change and intensification of coastal ocean upwelling. Science 247, 198–201.
Behrenfeld, M.J., O'Malley, R.T., Siegel, D.A., McClain, C.R., Sarmiento, J.L., 2006. Climate-driven trends in contemporary ocean productivity. Nature 444, 752–755, http://dx.doi.org/10.1038/nature05317.
Boyce, D.G., Lewis, M.R., Worm, B., 2010. Global phytoplankton decline over the past century. Nature 466, 591–596, http://dx.doi.org/10.1038/nature09268.
Chivers, S.J., Perryman, W.L., Kellar, N.M., Carretta, J.V., Archer, F.I., Redfern, J.V., Henry, A.E., Lynn, M.S., Hall, C., Jackson, A., Serra-Valente, G., Moore, T.J., Surrey-Marsden, C., Balance, L.T., 2010. Ecosystem Survey of *Delphinus* Species Cruise Report. NOAA Technical Memorandum NOAA-TM-NMFS-SWFSC-84.
Di Lorenzo, E., Miller, A.J., Schneider, N., McWilliams, J.C., 2005. The warming of the California Current system: dynamics and ecosystem implications. J. Phys. Oceanogr. 35, 336–362.
Djavidnia, S., Mélin, F., Hoepffner, N., 2010. Comparison of global ocean color data records. Ocean Sci. 6, 61–76, http://dx.doi.org/10.5194/os-6-61-2010.
Franz, B.A., Bailey, S.W., Werdell, P.J., McClain, C.R., 2007. Sensor-independent approach to the vicarious calibration of satellite ocean color radiometry. Appl. Opt. 46, 5068–5082.
García-Reyes, M., Largier, J., 2010. Observations of increased wind-driven coastal upwelling off central California. J. Geophys. Res. 115, C04011, http://dx.doi.org/10.1029/2009JC005576.
Gilbert, R.O., 1987. Statistical Methods for Environmental Pollution Monitoring. Van Nostrand Reinhold, New York.
Gregg, W.W., Conkright, M.E., 2001. Global seasonal climatologies of ocean chlorophyll: blending in situ and satellite data for the coastal zone color scanner era. J. Geophys. Res. 106 (C2), 2499–2516.
Gregg, W.W., Casey, N.W., O'Reilly, J.E., Esaias, W.E., 2009. An empirical approach to ocean color data: reducing bias and the need for post-launch radiometric re-calibration. Remote Sensing Environ. 113, 1598–1612, http://dx.doi.org/10.1016/j.rse.2009.03.005.
Gregg, W.W., Casey, N.W., 2010. Improving the consistency of ocean color data: a step toward climate data records. Geophys. Res. Lett. 37, L04605, http://dx.doi.org/10.1029/2009GL041893.
Henson, S.A., Sarmiento, J.L., Dunne, J.P., Bopp, L., Lima, I., Doney, S.C., John, J., Beaulieu, C., 2010. Detection of anthropogenic climate change in satellite records of ocean chlorophyll and productivity. Biogeosciences 7, 621–640.
IOCCG, 2007. Ocean-color data merging. In: Gregg, W. (Ed.), Report of the International Ocean-Color Coordinating Group, No. 6, IOCCG, Dartmouth, Canada.
Kahru, M., Mitchell, B.G., 1999. Empirical chlorophyll algorithm and preliminary SeaWiFS validation for the California Current. Int. J. Remote Sensing 20, 3423–3429.
Kahru, M., Mitchell, B.G., 2000. Influence of the 1997–98 El Niño on the surface chlorophyll in the California Current. Geophys. Res. Lett. 27, 2937–2940.
Kahru, M., Mitchell, B.G., 2001. Seasonal and nonseasonal variability of satellite-derived chlorophyll and colored dissolved organic matter concentration in the

California Current. J. Geophys. Res. 106, 2517–2529, http://dx.doi.org/10.1029/1999JC000094.
Kahru, M., Kudela, R., Manzano-Sarabia, M., Mitchell, B.G., 2009. Trends in primary production in the California Current detected with satellite data. Geophys. Res. Lett. 114, C02004.
Lorenzen, C.J., 1981. Chlorophyll b in the eastern North Pacific Ocean. Deep-Sea Res. 28, 1049–1056.
Lynn, R.J., Simpson, J.J., 1987. The California Current system: the seasonal variability of its physical characteristics. J. Geophys. Res. 92, 12947–12966.
Mackas, D.L., 2010. Does blending of chlorophyll data bias temporal trend? Nature 472, E4–E5, http://dx.doi.org/10.1038/nature09951.
Mantyla, A.W., Venrick, E.L., Hayward, T.L., 1995. Primary production and chlorophyll relationships, derived from ten years of CalCOFI measurements. Calif. Coop. Oceanic Fish. Invest. Rep. 36, 159–166.
Maritorena, S., Siegel, D.A., 2005. Consistent merging of satellite ocean color data sets using a bio-optical model. Remote Sensing Environ. 94, 429–440.
Maritorena, S., Fanton d'Andon, O.H., Mangin, A., Siegel, D.A., 2010. Merged satellite ocean color data products using a bio-optical model: characteristics, benefits and issues. Remote Sensing Environ. 114, 1791–1804.
Martinez, E., Antoine, D., D'Ortenzio, F., Gentili, B., 2009. Climate-driven basin scale decadal oscillations of oceanic phytoplankton. Science 326, 1253.
McClain, C.R., 2009. A decade of satellite ocean color observations. Annu. Rev. Mar. Sci. 1, 19–42.
McQuatters-Gollop, A., Reid, P.C., Edwards, M., Burkill, P.H., Castellani, C., Batten, S., Gieskes, W., Beare, D., Bidigare, R.R., Head, E., Johnson, R., Kahru, M., Koslow, J.A., Pena, A., 2011. Is there a decline in marine phytoplankton? Nature 472, E6–E7, http://dx.doi.org/10.1038/nature09950.
Morel, A., Antoine, D., 2007. Pigment Index Retrieval in Case 1 Waters. MERIS Level 2 Algorithm Theoretical Basis Document, ATBD2.9, ESA Doc. No. PO-TN-MEL-GS-0005 Issue 4.
Morel, A., Huot, Y., Gentili, B., Werdell, P.J., Hooker, S.B., Franz, B.A., 2007. Examining the consistency of products derived from various ocean color sensors in open ocean (Case 1) waters in the perspective of a multi-sensor approach. Remote Sensing Environ. 111, 69–88.
National Research Council, 2004. Climate Data Records From Environmental Satellites. The National Academies Press, Washington, D. C.
O'Reilly, J.E., Maritorena, S., Mitchell, B.G., Siegel, D.A., Carder, K.L., Garver, S.A., Kahru, M., McClain, C.R., 1998. Ocean color chlorophyll algorithms for SeaWiFS. J. Geophys. Res. 103, 24937–24953.
O'Reilly, J.E., 24 Coauthors, 2000. SeaWiFS Postlaunch Calibration and Validation Analyses, Part 3. Hooker, S.B., Firestone, E.R. (Eds.), NASA Tech. Memo. 2000-206892. NASA Goddard Space Flight Center, vol. 11, 49 pp.
Polovina, J.J., Howell, E.A., Abecassis, M., 2008. Ocean's least productive waters are expanding. Geophysical Res. Lett. 35, L03618, http://dx.doi.org/10.1029/2007GL031745.
Rykaczewski, R.R., Dunne, J.P., 2010. Enhanced nutrient supply to the California Current Ecosystem with global warming and increased stratification in an earth system model. Geophys. Res. Lett. 37, L21606, http://dx.doi.org/10.1029/2010GL045019.
Rykaczewski, R.R., Dunne, J.P., 2011. A measured look at ocean chlorophyll trends. Nature 472, E5–E6, http://dx.doi.org/10.1038/nature09952.
Salmi, T., Määttä, A., Anttila, P., Ruoho-Airola, T., Amnell, T., 2002. Detecting Trends of Annual Values of Atmospheric Pollutants by the Mann–Kendall Test and Sen's Slope Estimates—The Excel Template Application MAKESENS. Publications on Air Quality 31. ISBN 951-697-563-1. Report Code FMI-AQ-31, 35 pp.
Sen, P.K., 1968. Estimates of the regression coefficient based on Kendall's tau. J. Am. Stat. Assoc. 63, 1379–1389.
Werdell, P.J., Bailey, S.W., 2005. An improved in-situ bio-optical data set for ocean color algorithm development and satellite data product validation. Remote Sensing Environ. 98, 122–140, http://dx.doi.org/10.1016/j.rse.2005.07.001.